EMULSION SEPARATION AND FOULING OF ELECTROSPUN POLYACRYLONITRILE MEMBRANES FOR PRODUCED WATER APPLICATIONS

Separation and Purification Technology

Elizabeth M. Butler [1] and Jonathan A. Brant [1,*]

[1] University of Wyoming, department of Civil and Architectural Engineering and Construction Management, 1000 E. University Avenue, Laramie, WY, 82071.

* Corresponding author. Email: jbrant1@uwyo.edu.

September 13, 2022

ABSTRACT

Produced water (PW) is a complex mixture generated during oil and gas extraction. Membrane fouling by hydrocarbon emulsions (sizes <10 μm) challenges most PW treatment systems. Electrospinning has the possibility of creating microporous membranes that present unique performance properties, though evaluations of these characteristics are largely restricted to unrealistic dead-end configurations. Three different nanofibrous polyacrylonitrile (PAN) membranes were synthesized by electrospinning and their performances contrasted with a commercially available PAN membrane. Feed solutions included synthetic oil and solvent emulsions and a produced water from an operating well-site. Two nanoparticles, polyaniline (PANI) and reduced graphene oxide (RGO), were studied for enhancing the oleophobicity and fouling properties of the electrospun PAN membranes. Electrospun membranes showed higher porosities (68 to 80%) and water permeance values (9,000 to 10,000 LMH/bar) relative to that for the commercially available PAN membrane (44% and 8,800 LMH/bar). All electrospun membranes provided superior performance characteristics when treating the emulsions and produced water relative to the commercial membrane. The PANI integrated membrane demonstrated the greatest resistance to oil/solvent emulsion fouling and comparable performance to the RGO and PAN membrane treating the produced water.

Keywords: Produced water, oil and grease fouling, electrospinning, filtration.

1. INTRODUCTION

Produced water (PW), which is a mixture of formation water and if used, hydraulic fracturing fluids [1], has garnered much interest from diverse stakeholders. These interests stem from reducing the environmental footprint of the energy industry, improving the economics of resource extraction, and recovering the many resources contained in PWs, like critical minerals. For context, approximately ~24.4 billion barrels (~3.8 billion cubic meters) of PW was generated in the U.S. in 2017 [2]. Of this volume less than 3% was beneficially reused [2]. The remaining fraction was disposed of through reinjection wells or surface impoundments (evaporation ponds). Challenging reuse applications is the lack of economically viable treatment processes capable of accommodating the complex and dynamic characteristics of PWs. Common PW constituents include salts, oils and greases (O&G), hydrocarbons, minerals/metals, and organics that may be added as part of hydraulic fracturing processes [1]. Developing treatment systems that can accommodate such complex and variable compositions continues to challenge stakeholders.

A common constituent of PWs produced from conventional, and unconventional, wells are O&G. Fractions of O&G, typically emulsions of small size fractions, persist in the PW at relatively high concentrations (~170 to 4,000 mg/L) after passing through separation processes, like hydrocyclones and/or gun barrel separators (a series of settling and wash tanks) [3, 4]. This persistence is due to the inability of many separation processes to remove the smaller size fractions of emulsions. For example, hydrocyclones are only effective at removing emulsions with a size ≥ 10 μm [5]. Microfiltration (MF) and ultrafiltration (UF) membranes have been used to achieve greater than 90% separation of oil emulsions with sizes <10 μm [6, 7]; however, fouling remains a major hurdle for these processes [8-10]. Many studies have shown that compared to other substances, O&G fouling occurs in unique ways, such as coalescing and deforming to enter and constrict/block membrane pores [10-15]. Oil droplets are carried toward the membrane surface in crossflow filtration due to filtrate drag forces. The deposited droplets begin to block membrane pores [10]. As more oil droplets begin to attach on the membrane surface, a gel layer

is formed decreasing water permeation [16, 17]. Due to the malleability of oil droplets, the gel layer can become dense (high hydraulic resistance) or even enter the pore throats resulting in severe flux loss [12]. Interfacial interactions, originating from electrostatic, van der Waals and Lewis acid-base interactions (hydrophobicity/hydrophilicity), play an important role in determining the rates and severity of these fouling mechanisms [12, 18]. Therefore, creating membrane surfaces that present unfavorable interaction scenarios for O&G fouling are needed.

Creating membranes that are resistant to O&G fouling has largely been pursued by through the development of hydrophilic and superhydrophilic polymers [19, 20]. The term superhydrophilic refers to a surface with a contact angle with water of <5-10° [21], which implies a high affinity for water and in turn a low affinity for non-polar substances, like O&G. The favorable interaction with water arises from the prevalence of Lewis acid-base sites that are present on the polymers that make up the membrane surface [22]. In general, superhydrophilic membranes have been shown to be more resistant to O&G fouling relative to more conventional ones [23, 24]. Further, superhydrophilic membranes have been shown to achieve O&G separation efficiencies of >99% [19, 20, 25], indicating that the O&G does not penetrate and pass through the membrane pores. Synthesizing superhydrophilic membranes can be done through grafting of hydrophilic materials to a polymeric substrate, incorporation of nanoparticles into or on the membrane matrix, and/or coating of the membrane surface with hydrophilic polymers. Electrospinning/spraying is another method that is receiving interest as a means for creating membranes for O&G separation [26, 27]. This interest is due to the ability to tightly control the physical and surface chemical properties of the produced nanofibers and in turn those of the membrane.

Electrospinning is a process by which nano-fibers are formed when a polymer/solvent solution is injected into an electric field that exists between an emitter (needle) and a target (collector surface) [28]. The characteristics of the nanofibers are a function of the environmental conditions (temperature, humidity) in the chamber and the polymer solution chemistry (electrical conductivity, viscosity). Other process parameters that must be considered include the distance and voltage

gradient between the emitter and the target. Electrospun membranes are a potentially attractive option for membrane synthesis due to the ability to form high-porosity, low-tortuosity microporous membranes, while also being able to integrate nanomaterials into the nanofibrous matrix [5]. Because the nanofibers are formed nearly instantly the nanomaterials do not suffer from aggregation, as in conventional polymerization processes. This characteristic minimizes the formation of defects within the membrane structure. Incorporation of nano-additives into the membrane material matrix allows for the creation of superhydrophilic, as well as other fouling resistant, surfaces. The addition of polyaniline (PANI) [27] and reduced graphene oxide (RGO) [29] have been used to increase the hydrophilicity of electrospun polyacrylonitrile (PAN) nanofibers. PANI/PAN and RGO/PAN blended membranes have been shown to be effective in oil/water separation applications [30, 31]; however, these studies have been restricted to dead-end configurations that are not representative of the conditions used in commercial membrane systems.

The objective of this study was to assess the performance of a commercially available PAN MF membrane against two electrospun membranes, which were modified using PANI and RGO to enhance their hydrophilicity, for separating non-aqueous phases (hydrocarbons) from water. Mixtures were made to represent that of oil and gas PW, in addition to PW that was collected from an active oil and gas well-site in Greater Green River Basin (GGRB) in Wyoming. Membrane performance was evaluated in a crossflow configuration, which to our knowledge has been minimally explored in the literature. Membrane synthesis conditions were optimized to maximize hydrophilicity, antifouling properties, and O&G rejection, which were correlated by membrane characteristics of pore size, porosity, and surface chemistry

3. EXPERIMENTAL

3.1 Chemicals and Reagents

Polyacrylonitrile (PAN) (average M_w = 150,000), ammonium peroxodisulfate (APS), Kaolin clay, and reduced graphene oxide (RGO) (Carbon>75%, Oxygen<22%) were purchased from

Sigma-Aldrich, USA. Aniline (99.8% purity), N,N-dimethylformamide (DMF) (certified ACS grade, >99.9%), sodium bicarbonate, sodium chloride, 10M sodium hydroxide, and 10M hydrochloric acid were acquired from Fisher Scientific (Pittsburg, PA). The following solvents and oil were used in the membrane performance analyses light mineral (paraffin) oil (Fisher Scientific), benzene (purity≥99.9%, Sigma-Aldrich), and toluene (purity≥99.8%, Fisher Scientific). All model test solutions were made using ultrapure water having a resistivity of 18 MΩ·cm and an unmodified pH=6.4.

3.2 Characterization of Produced Water (PW) Samples

The total oil and grease (O&G) concentration in PW samples was measured according to Standard Method 5520B. The following solids analyses were done according to Standard Method 2540: total solids (TS), total suspended solids (TSS), and total dissolved solids (TDS). Turbidity was measured using a Hach 2100Q Portable Turbidimeter (Hach, Loveland, CO). Solution pH and electrical conductivity were measured using a Accumet XL200 (Fisher Scientific, Pittsburgh, PA) benchtop meter.

3.3 PW Source and Characteristics

PW samples were collected from a field site in 60 L plastic containers and then stored at 5°C until used. No biocides or other stabilizing agents were added to the PW samples during storage. For those samples collected from a point-source (tap) the line was flushed for several minutes prior to collecting the sample for testing. This was done to avoid collecting substances and microbiological components that may collect over time at the sampling valve. This PW source immediately followed the gun barrel and prior to disposal through reinjection. The grit content of the PW was approximately 110 mg/L. Grit was removed from the PW samples prior to testing by quiescent settling. This PW was much more saline $(3\times)$ that of the average TDS concentration for GGRB PWs with a mean TDS concentration of 76,140 mg/L. Average GGRB total O&G and TDS concentrations values were 2,500 mg/L and 23,800 mg/L, respectively [3]. The PW tested

here was characterized by a high TSS concentration (172 mg/L), near neutral pH (7.5), and a total O&G concentration of 4,725 mg/L.

3.3 Membrane Synthesis

3.3.1 Polymer Solution Preparation for Membrane Synthesis

Polyaniline (PANI) has been shown to increase nanofiber hydrophilicity due to the amino groups that are present along the PANI molecular chain, in addition to the roughness features that it imparts onto electrospun nanofibers [27, 32]. Several studies have shown PANI to be effective in increasing membrane hydrophilicity and oil rejection [27, 30, 32-34]. For this reason, PANI, in addition to RG), was evaluated for improving the performance of the PAN membranes. PANI was made according to the procedure published by Shakiba, et.al.[30]. Solutions of aniline (0.84 M) and APS (0.84 M) were separately prepared by dissolving them in 0.64 M hydrochloric acid at 20°C. Solutions were hand shaken for 30 sec. The APS solution was added to the aniline solution in a jacketed reactor that was agitated using an impeller mixer. The mixture was maintained in a nitrogen atmosphere at 0°C for 2 hrs. The mixture was then centrifuged at 5000 rpm for 10 min to separate the PANI precipitate from the suspension. The precipitate was rinsed with ultrapure water, then ethanol, and lastly with ultrapure water. The mixture was centrifuged after each rinse at 5000 rpm for 10 min. The PANI paste was dried at 50°C for 24 hr. The dried PANI powered was milled in a high energy micro-vibrational mill (MSK-SFM-12M by MTI Corporation) at 3000 rpm for 60 sec to improve its dispersion in DMF.

Graphene oxide (GO) is a 2D material composed of oxidized graphene sheets where epoxide, hydroxyl, carbonyl and carboxyl groups are formed on the graphite lattice [35]. These oxygenated groups make GO highly hydrophilic and it disperses easily in polar solvents [36]. Reduced graphene oxide (RGO) partially removes these oxygenated groups reducing its hydrophilicity due to the loss of surface polarity [37, 38] which is expected to improve its dispersion in DMF, It was therefore selected for study as an additive to the PAN membranes to both enhance water flux and to improve the fouling resistance of the electrospun membranes. RGO powder was milled in a

high energy micro-vibrational mill (MSK-SFM-12M by MTI Corporation) at 3000 rpm for 60 sec to reduce the discrete particle size. After milling, the RGO had a mean particle size of 300 nm in DMF as determined from dynamic lightering measurements. This was an important processing step as larger particle sizes can result in needle plugging during the electrospinning process, as well as settling in the solvent/polymer solution.

PAN was selected for forming the hydrophilic nanofibrous membranes as it has been shown to be effective in oil/water separation applications [27, 39]. Solutions of 4%, 6%, 8%, 10% and 12% (w/w) PAN in DMF were prepared by stirring with an impeller mixer at 650 rpm for 12 hrs. After mixing, the solution was bath sonicated (Branson 5800) for 60 min to remove air bubbles and ensure complete dissolution of the PAN. A 3.5% (w/w) PANI in DMF solution was hand shaken, bath sonicated for 12 hr, and then probe sonicated (Sonic Dismembrator Model 500, Fisher Scientific) at 20% amplitude for 15 min. A PANI/PAN/DMF solution was made by adding the PANI/DMF solution to a 12% (w/w) PAN/DMF solution to achieve a 30% (w/w) PANI to PAN in 6% (w/w) PAN to DMF solution and mixed for 4 hrs at 650 rpm. Shakiba et al. found that a 30%PANI/PAN concentration had the highest oil rejection of PANI/PAN membranes spun at ambient temperatures [30]. A 0.8% (w/w) RGO in DMF solution was hand shaken, bath sonicated for 12 hr, then probe sonicated at 20% amplitude for 15 min. RGO/PAN/DMF solutions were made by adding the RGO/DMF solution to a 12% (w/w) PAN/DMF solution to achieve a 7% (w/w) RGO/PAN in 6% (w/w) PAN to DMF and mixed for 4 hr at 650 rpm. A 7% RGO/PAN solution was studied based on Zhang et. al's research showing increased oil selectivity for membranes made using this additive/polymer ration [29]. PANI and RGO solutions were given 24 hr after mixing to settle any large undissolved PANI or RGO before spinning.

3.3.3 Fabrication of PAN, PANI/PAN, RGO/PAN Membranes

All electrospun membranes were formed on Cranemat RS 15.5 (CM 15.5), which is a nonwoven polyethylene terephthalate (PET) fabric (Neenah Filtration, Pittsfield, MA). The CM 15.5 had a mean thickness of 0.109 mm and a nominal pore size of 20 μm.

Electrospinning/spraying tests were done using a pilot-scale electrospinning system (Fluidnatek LE-500, Nanoscience, Phoenix, AZ) that was integrated with an environmental control unit that controlled temperature, relative humidity (RH), and the exchange of air within the electrospinning chamber. The LE 500 was equipped with three power supplies: two high-voltage sources capable of operating up to +50 kV and a grounded target capable of operating down to -15 kV. Polymer solutions were delivered to the target via computer-controlled syringe pumps. Other process parameters, such as roller speed, *x*-, *y*-, *z*-position of the solution emitter(s) and scanning speed of the emitter(s) were controlled via the programmable logic controller. Roll-to-roll production of membrane samples could be done by rolling the membrane substrate across the flat stainless steel plate collector at a set speed and solution flowrate to achieve a given unit mass deposition (g/m^2) that correlated to a given membrane thickness. Temperature [40] and RH [41] within the spinning chamber are known to affect the sizes and surface textures of the produced nanofibers, as well as the pore size of the resultant membranes. Warmer spinning temperatures create thinner, more fragile fibers with smaller pore sizes [40]. Increased RH increases surface roughness and decreases tensile strength in PAN [41]. Therefore, these conditions, in addition to solution flowrate and emitter to target distance, were optimized prior to membrane production.

Polymer solutions were made and then loaded into polypropylene syringes (inner diameter = 20.05 mm), which incorporated a 22-gauge needle. Pertinent electrospinning process variables are summarized in **Table S1**. Syringes were degassed by placing the syringe in a plastic bag in a bath sonicator (Branson 5800) for 15 min immediately prior to electrospinning to ensure complete removal of air bubbles that could interfere with cone stability. All PAN solutions were spun at a RH of 22% based on Szewczyk and Stachewicz's findings showing PAN fibers spun at 22% were characterized by the highest tensile strength relative to PAN nanofibers spun at other RHs [41]. All membranes were spun at a needle tip to collector distance of 14 cm and a solution flowrate of 1 mL/hr. Membranes used for filtrations testing were made in two layers. The total

voltage gradient between the emitter and the collector was varied from 14 to 17 kV, with the target voltage maintained at -2 kV.

A control membrane made of PAN, referenced here as Base_PAN, was made to elucidate the abilities of RGO and PANI to improve the performance of the PAN membrane for treating the PW. The separating layer for Base_PAN, RGO_PAN, and PANI_PAN all used 6% PAN solution base to achieve the desired nominal pore size for the membrane. All membranes were made by first applying a coating of 12% PAN on the CM 15.5 followed by the formation of the 6% PAN separating layer. The purpose of the 12% PAN coating was to increase the mechanical strength and adhesion of the composite PAN membrane to the CM 15.5. This step was pursued based on observed delamination of the PAN nanofibers made using lower polymer concentrations from the substrate. The 12% PAN solution was spun with a voltage difference of 14 kV at 25°C on to the CM 15.5 substrate for 3 hrs over an area of 650 cm^2 to achieve a desired thickness of 40 μm. The topcoat was immediately applied following of the 12% PAN coating to reduce the potential for membrane damage between coats. A 6% PAN, PANI/PAN, or RGO/PAN solution was spun on top of the 12% PAN with a voltage difference of 16 kV and at 30°C for 12 hrs over area of 650 cm^2 to achieve a desired thickness of 150 μm. Membranes were in ultrapure water until tested.

3.4 Membrane Morphological Analyses

Membrane surface morphology was characterized using field emission scanning electron microscopy (FESEM, FEI Quanta FEG 450, Thermo Fisher Scientific, USA) with an accelerating voltage of 5 kV. Prior to FESEM imaging, membrane samples were prepared with a carbon coating using a vacuum sputter-coating system to prevent charge accumulation during imaging. Representative FESEM images were acquired by scanning samples from 3 different runs and taking images of each sample. The height of formed nanofibrous layers and nanofiber diameters were evaluated using a 3D laser scanning microscope (VK-X1000, Keyence, USA) and the profile tool on the Keyence Multifile Analyzer program. The VK-X1000 has a vertical resolution of 20 nm and lateral resolution of 50x50 mm. The image analysis software allows for the determination of

line and surface roughness of flat or curved surfaces, radii of curvature, step heights, and pore volume and surface area. Reported thickness and nanofiber diameters represent the mean of a minimum of 15 heights and 75 fiber diameters for each membrane. The laser scanning microscope was also used to characterize the morphologies of foulant layers formed on the membranes when treating oil/water mixtures and PW samples.

3.5 Characterization of Membrane Physical Properties

Membrane pore size was determined using a gas-liquid porometer (Porolux1000, Porometer, Germany). Perfluoroether (Porefil, Porolux) was used as a wetting liquid due to its low vapor pressure (399 Pa) and low surface tension (16.4 mN/m), which ensured complete wetting of membrane surfaces and pores. A pore shape factor of 0.75 was assumed for all membranes for calculating pore size. A minimum of 5 samples per membrane were used to determine mean pore size values. Mean free pore (MFP) size was collected and reported. MFP refers to the pore size at which 50% of the total gas flow has occurred. Membrane porosity was determined using the gravimetric approach, as described in **Eq. 1** [42].

$$\varepsilon(\%) = \frac{W_w - W_d}{\rho_w V} \times 100 \qquad \textbf{Eq. 1}$$

where W_W and W_d are the wet and dry weights of the membrane respectively, ρ_w is the density of ultrapure water at 22°C at which the tests were done (= 0.99777g/cm^3), V is the volume of the membrane. The volume was calculated by multiplying the coupon area by the thickness measured on the laser scanning microscope. A minimum of 9 samples were tested for each membrane to calculate average porosity.

3.6 Characterization of Membrane Surface Chemistry

Membrane hydrophilicity and hydrophobicity were assessed in terms of a measured Young's contact angle, θ_Y. Generally, surfaces with θ_Y<90° are characterized as hydrophilic, while surfaces with θ_Y>90° are defined as hydrophobic. Surfaces with θ_Y<10° are characterized as being superhydrophilic and those with θ_Y>150° are superhydrophobic [21]. Contact angles are

related to the interfacial energies that exist between the membrane, water and air at the three-phase boundary as described by Young's equation (**Eq. 2)** [43]:

$$\gamma_{LV}\cos\theta_Y = \gamma_{SV} - \gamma_{SL} \quad \textbf{Eq. 2}$$

where γ_{SV} is the solid–vapor surface energy, γ_{SL} is the solid–liquid surface energy, and γ_{LV} is liquid–vapor surface energy. Young's equation assumes a homogenous, rigid, and flat solid surface, which is often not characteristic of microporous membrane surfaces. Therefore, the captive bubble technique was used for all contact angle measurements done using a goniometer (EasyDrop, Krüss Scientific, Hamburg, Germany). Captive bubble measurements were conducted considering the high porosities that characterized the membranes and the propensity of water to quickly permeate into the material matrix when using the sessile drop technique. For the captive bubble measurements, the membrane coupon was loaded onto a stage and tension applied using a screw stage to reduce sample curvature effects. A U-shaped needle was submerged in ultrapure water contained in a quartz cell below the membrane to release a bubble with a volume 2 µL onto the membrane surface. Captive bubble measurements were taken with air, mineral oil, toluene, and benzene. Contact angles of the tested solvents/oils on the membrane surfaces were measured using the captive bubble technique. The contact angle was determined as the angle measured through the solvent/oil phase. All measurements were done at ambient temperature (20°C). Reported values, calculated as the average of the left and right contact angle, represent the mean value of a minimum of nine different measurements (3 bubbles/droplets per sample and a total of 3 samples).

3.7 Assessment of Membrane Performance

Synthesized PAN membrane performance was compared to that of a commercially available PAN membrane (PAN022005, Sterlitech Corporation, Kent, WA) having a reported nominal pore size of 0.2 µm. This membrane was designated as COM_PAN. The COM_PAN membrane was constructed of PAN nanofibers laminated on PET support substrate for a total thickness of 180 to 200 µm with a max operation temp of 90°C as reported by the manufacturer. COM_PAN is used

in a wide variety of filtration applications with recommended uses including drinking water applications, fluid purification for industrial processes, food and beverage filtrations, and biopharmaceutical processing. This commercial membrane was selected for comparison due to having the same material composition and similar pore size to Base_PAN. Membrane performance was evaluated in terms of water flux (LMH), permeance (LMH/bar), phase rejection, and fouling (flux decline). Permeance was assessed using a dead-end filtration system, while water flux and membrane fouling were characterized using a crossflow system. The process flow diagrams of both systems are shown in **Figure S1**. Membrane permeance (LMH/bar) was measured using a dead-end filtration cell (HP4750, Sterlitech Corporation) having an active membrane area of 14.6 cm^2. Permeance measurements were done using ultrapure water as the feed solution. Pressure was supplied using a compressed nitrogen gas cylinder and a dual stage pressure regulator. Water flux and feed pressure were digitally recorded respectively through a computer interfaced mass balance and pressure sensor. Permeance was calculated by varying the backpressure over a range of 0.2 to 0.55 bar using ultrapure water as the feed solution. Flux was recorded at each pressure step for 15 mins per step, held at 0.55 bar for 3 hrs and then the process was repeated by decreasing the decreasing pressure step to evaluate for membrane compression. The permeance was calculated as the slope from a linear regression analysis of flux as a function of pressure.

For the crossflow experiments membrane samples were housed in a cross-flow cell (CF042D, Sterlitech Corporation) having an active area of 42 cm^2 and slot dimensions of 2.28 mm (depth) and39 mm (width). All tests used a high-foulant PTFE spacer (thickness = 55 mil, Sterlitech Corporation) and a crossflow velocity of 30.0 cm/sec. All membrane samples were hydrated for ≥24 hrs in ultrapure water prior to testing. Model solvent/oil tests were evaluated using were assessed using a background electrolyte solution (TDS=20,000 mg/L NaCl, pH=7) with mineral oil (5% V/V), toluene (1 and 2% V/V), or benzene (1% V/V) added to form an emulsion. The background electrolyte solution used a TDS concentration to approximate that of average PW.

The membrane performance was first evaluated with the background electrolyte solution for 1 hr at a backpressure of 0.35 bar. Phase selectivity and membrane fouling were evaluated using the same initial filtrate flux (1300 LMH) and flowrate (~90 mL/min) to avoid discrepancies associated with varying initial permeate drag forces and to reduce the overall drag forces on the foulants. Tests were maintained at a backpressure of 0.35 bar.

Membrane performance was also assessed using field collected PW samples. Performance tests using the PW as a feed solution were done without altering, or pretreating, the sample, except for grit removal via clarification for 30 min and decanting. Each test employed a solution volume of 4 L so that the composition of the feed mixture remained relatively constant through the duration of a given tests when filtrate samples were removed and analyzed. The initial filtrate flux (~1300 LMH) and feed pressure (0.35 bar) were the same as those used in the model solution tests.

Oil/solvent and particulate rejection were quantified by measuring the turbidity of feed and filtrate samples using a turbidimeter (Model: 2100Q, Hach, Loveland, Colorado). Filtrate and feed samples were collected periodically throughout each test, analyzed for turbidity, and then returned to the feed reservoir. Water flux, measured using a computer interfaced mass balance, was recorded until a quasi-steady-state value was achieved to characterize membrane fouling (flux decline). Post-test fouling was observed using a 3D laser scanning microscope (VK-X1000, Keyence, USA).

Emulsions are not rigid and may deform to enter, and pass through, pores of comparatively smaller sizes [11, 12, 44, 45]. For emulsions, pore size must be considered in combination with hydraulic drag and lift forces, in addition to interfacial chemical interactions when assessing phase rejection/permeation. As shown in **Figure S2**, an oil droplet may deform to penetrate a pore of a membranes with diameter smaller than that of the droplet diameter [46]. Such penetration is less favorable for hydrophilic/oleophobic surfaces due to repulsive electrostatic interfacial interactions between the hydrophobic droplet and the hydrophilic membrane surface [19]. The hydraulic

pressure required for a given phase to enter a pore throat, defined as the critical entry pressure, ΔP_{crit} may be quantified according to the energy balance shown in **Figure S2**. The forces acting on the oil droplet in **Figure S2** for a crossflow system are the filtrate drag, the cross-flow shear, hydraulic pressure, the oil/water interfacial tension/energy, and membrane/oil interfacial tension/energy. These forces dictate oil attachment, pore penetration, oil breakthrough, and oil detachment. For hydrophilic/oleophobic (θ_{WO} < 90°) membranes, ΔP_{crit} can be described by **Eq. 3** [47].

$$\Delta P_{crit} = \frac{2\gamma_{WO}cos\theta_{WO}}{r_{pore}}\left[1 - \left(\frac{2 + 3cos\theta_{wo} - cos^3\theta_{WO}}{4\left(\frac{r_{drop}}{r_{pore}}\right)^3 cos^3\theta_{WO} - \left(2 - 3sin\theta_{WO} + sin^3\theta_{WO}\right)}\right)^{\frac{1}{3}}\right] \quad \textbf{Eq. 3}$$

where r_{pore} is the pore radius, γ_{WO} is the oil/water interfacial tension/energy, and θ_{WO} = 180°-θ_{OW}, where θ_{OW} is the contact angle of oil on the membrane surface and θ_{WO} is the contact angle of the water on the membrane surface in the presence of oil droplet. While θ_Y defines the hydrophilicity of the membrane, θ_Y does not capture the solid/oil and oil/water interfacial interactions. To determine the membrane's oleophobicity, θ_{OW} was measured. Interfacial tension/energy values for the tested solvents/oils and water were taken from van Oss [43] and are summarized in **Table S2**.

4. RESULTS AND DISCUSSION

4.1 Membrane Characteristics

Nanofiber diameter was an important characteristic as it affects the pore size of the resultant membrane [40]. The objective in this study was to achieve a membrane with a nominal pore size of ~0.5 µm, which represented a moderately tight microfiltration (MF) membrane. Nanofiber diameter decreased with decreasing solution viscosity (**Figure S3**), in accordance with changes in polymer concentration and temperature, which affect solution viscosity and solvent evaporation

rate, respectively [48]. FESEM images (**Figure 2**) of the associated membranes corroborated expectations that the reduction in nanofiber diameter correlated to a decrease in pore size (**Figure 1)**; however, at a concentration of 4%PAN, the synthesis conditions were a mix of electrospinning of and electrospraying as evidenced by incomplete fiber formation and polymer balling. This resulted in a fragile material that easily degraded when handled and was therefore not feasible for membrane synthesis. Therefore, 6%PAN was selected for further testing, to include serving as the base material for the RGO and PANI modified membranes. The 6%PAN solution produced membranes having an MFP = 0.5-0.6µm.

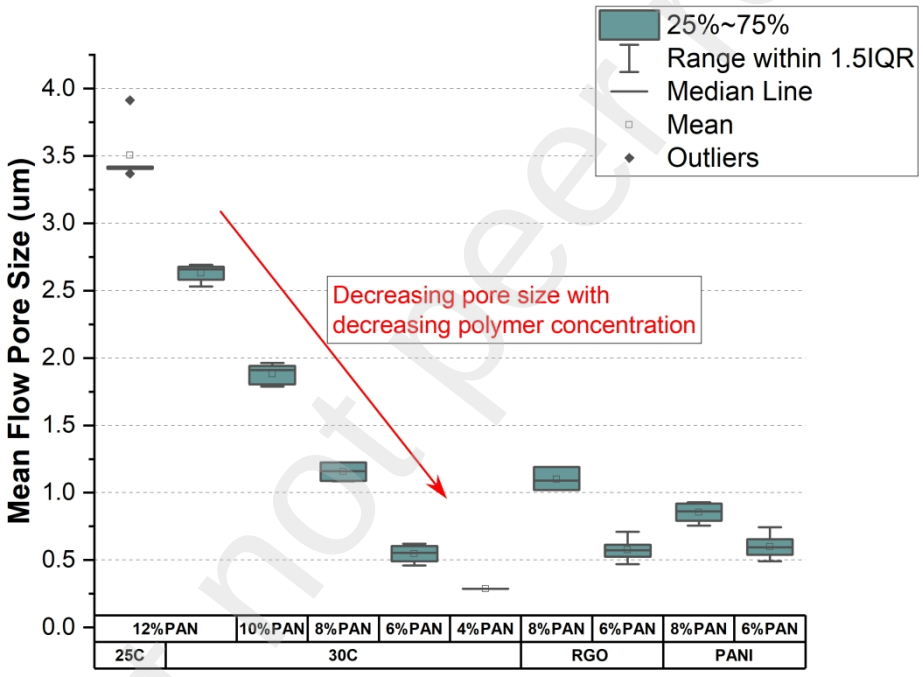

Figure 1. MFP size (µm) for the different temperature and PAN concentrations evaluated for synthesizing the nanofibrous membranes (RH = 22%, Spinning Distance = 14 cm, FR = 1 mL/hr).

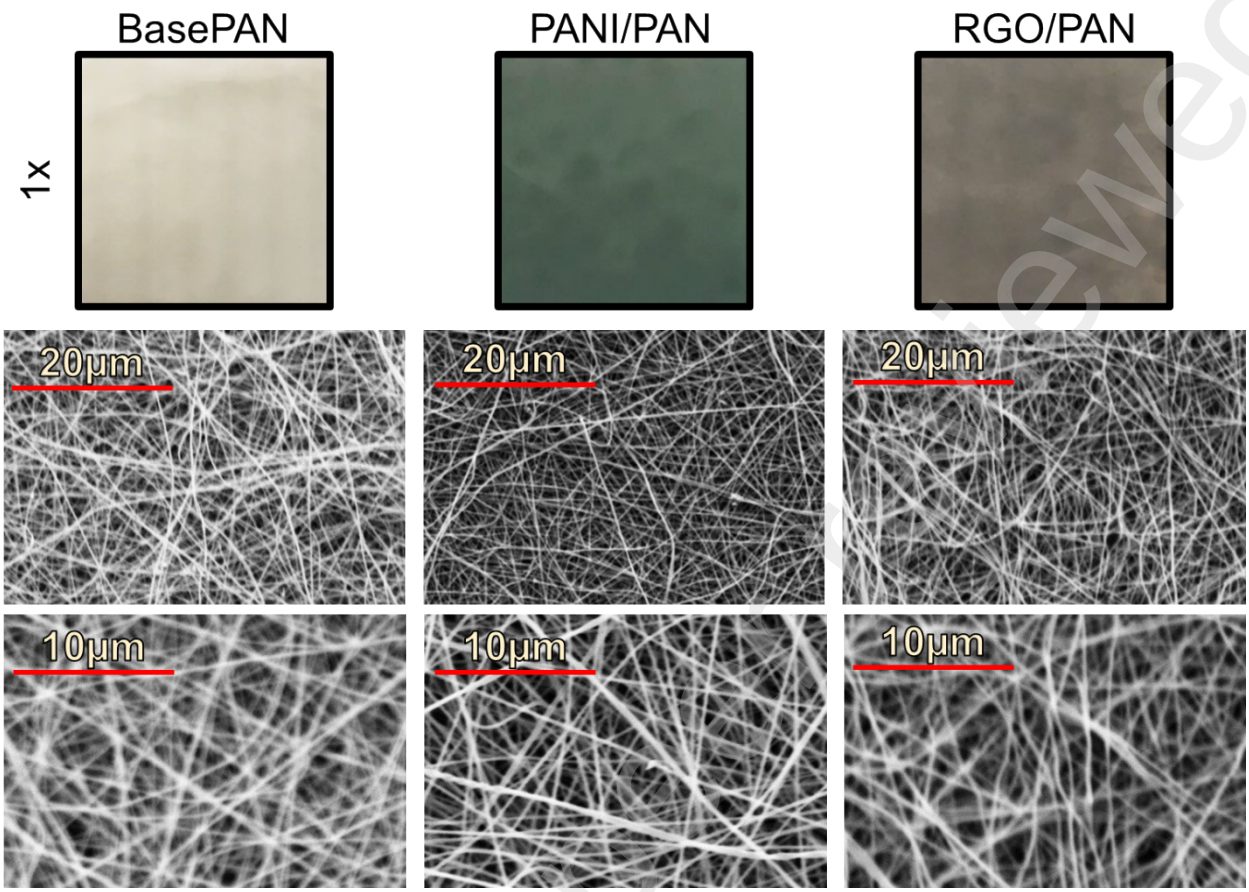

Figure 2. (*top*) Optical images of the BasePAN, PANI/PAN, and RGO/PAN membranes. The membranes are distinguished by their coloring going from white for PAN, green for the PANI, and grey for the RGO that was integrated into the PAN nanofibrous matrix. (*bottom*) FESEM images of the BasePAN, PANI/PAN, and RGO/PAN nanofibrous membranes.

Relevant physical characteristics of all 6% PAN membranes are summarized in **Table 1**. The mass loadings of PANI and RGO onto the PAN substrates were approximately 3.5 g/m^2 and 0.7 g/m^2, respectively, based on their concentrations in the spinning solution, spinning time, and membrane area covered. These mass loadings were selected based on the ability to form a stable dispersion of the nanomaterials in the DMF/PAN mixture to prevent aggregation and the formation of physical defects in the formed PAN nanofibrous layers. Physical defects for higher mass loadings were evidenced by the aggregation, or clumping, of the associated nanomaterials in the formed membrane. As shown in **Figure 1**, the addition of the PANI or RGO did not increase the

measured membrane pore size and indicates that the nano-additives did not result in defect formation. The presence of PANI and RGO in the nanofibrous structure were visually confirmed through the change in membrane color from white to green (PANI) or grey (RGO) (**Figure 2**). A previous work on PAN_PANI membranes had determined that the PANI adsorbs to the PAN nanofiber surface through hydrogen bonding between the di-amine and diimine groups of the aniline and the nitrile group of PAN [27]. As shown in this previous effort the PANI increased the surface roughness of the PAN nanofibers. The increase in fiber roughness was cited as a reason for making the nanofibers superhydrophilic based on contact angle analyses.

Table 1. Summary of polyester substrate and PAN membrane characteristics.

Membrane	Coverage (g/m^2)	Fiber Diameter (nm)	Thickness[1] (μm)	Porosity[3] (%)	MFP (μm)	Permeance (LMH/bar)
CM 15.5	59.7	-	100	29.1	21.9	36,821±3,521
COM_PAN[2]	4.0±0.8	-	180-200	44.7±7.4	0.52±0.02	8,830±54
Base_PAN	13.8±5.6	193±60	183.3±43.0	68.6±10.9	0.55±0.08	9,727±42
RGO_PAN	13.9±5.3	189±60	166.9±25.8	77.7±13.5	0.58±0.07	9,608±64
PANI_PAN	13.9±3.5	198±60	174.6±19.2	80.2±11.1	0.60±0.07	10,002±58

1. Thickness corresponds to total membrane thickness (12%+6% PAN) without CM 15.5 support layer.
2. COM-PAN thickness and nominal pore size of 0.2μm commercially reported. Coverage, MFP, porosityand permeance determined experimentally.
3. Reported porosity values are for the active nanofibrous layer(s) and do not account for the CM 15.5 support.

Captive bubble contact angle measurements were done to assess the relative hydrophilicity of the different PAN membranes (**Figure 3**). All membranes were characterized by statistically similar contact angles, indicating that they all were similarly hydrophilic. Note that the polyester substrate (Cranemat 15.5) was hydrophobic ($\theta_Y \approx 124°$). There was a general trend of the electrospun membranes being more hydrophilic, with the RGO_PAN membrane displaying a higher affinity for water than the other membranes. Regardless, the synthesized membranes were all characterized as highly hydrophilic, though not meeting the characteristic of superhydrophilic ($\theta_Y \leq 10°$) based on the captive bubble measurements. Of note, however, is that all the

synthesized membranes were characterized by contact angles with water of approximately 0° when measured using the sessile drop technique.

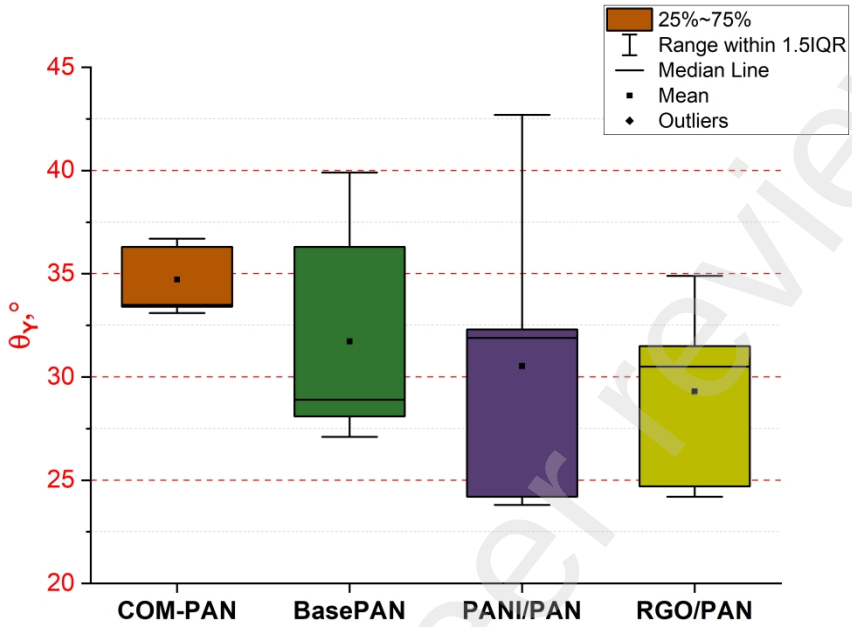

Figure 3. Mean captive bubble contact angle with water results (black square symbol) for the commercial PAN and the synthesized nanofibrous PAN membranes ($\boldsymbol{V_D = 2\mu L}$; pH=6.4, *T*=20°C, *n*=9).

The permeance of the PAN nanofibrous membranes was lower than that of the CM 15.5 substrate (**Table 1**). This was due to the formation of the nanofibrous layers, or mats, on the macroporous substrate having a hydraulic permeability lower than the substrate. Each of the nanofibrous membranes was characterized by a higher permeance than the commercially available PAN membrane. Although this may be attributed to differences in pore size, it must be recognized that when subjected to porometry measurements the measured MFP for the commercial membrane (MFP=0.52±0.02 µm) was comparable to the nanofibrous ones (**Table 1**). Therefore, higher porosities, and lower pore turtuosities, for the nanofibrous membranes may be playing a significant role. The porosities of the synthesized PAN membranes were between 135% to 144% that of the COM_PAN membrane. Porosities were marginally higher for the PANI (144%)

and RGO (142%) membranes than that of the Base_PAN membrane (135%); however, this did not translate into substantially higher permeance values (**Table 1**). At the hydraulic pressure gradients used here (≤ 1 bar) it is not likely that water transport through the nanoporous RGO would have been significant. Further, the PANI was present on the nanofibers in the form of discrete roughness structures rather than permeable media. Therefore, neither additives were likely to form preferential flow paths for water. Rather, both enhanced the hydrophilicity of the overall structure and in turn the affinities of the membrane material for water. The permeance values reported here for the three synthesized PAN membranes fell within the range of other reported values for electrospun PAN membranes (2,200-35,000 LMH/bar) [27, 29, 49]. This large range in reported values may be attributed to differences in membrane pore size and thicknesses across the different electrospinning studies.

4.2 Membrane Performance and Fouling

4.2.1 Solvent Permeation and Membrane Fouling Assessment

Crossflow experiments using various aqueous mixtures of organic solvents and mineral oil were executed to evaluate the permeation/rejection of the solvent emulsions and characterize membrane fouling by the relevant solvents. Flux as a function of filtration time for each of the tested membranes when treating mixtures of mineral oil, toluene and benzene are respectively summarized in **Figures 4**, **5**, and **6**. Of note, the starting flux for the mineral oil test (~5,600 LMH) was higher than that used for the other solvents (~1,300 LMH). No filtrate throttling was done for the mineral oil because no fouling was observed for any of the membranes at the lower flux. This was attributed to the oil's lower density (**Table S2**) and in turn it not being subject to sufficient drag forces to rapidly foul the membranes. Associated filtrate turbidity values are also reported. When treating the mineral oil emulsion, the PANI_PAN membrane was characterized by the least amount of flux loss (~5%), while the other PAN membranes were characterized by similar flux decline profiles and flux loss values (~15 to 22%). For each of the membranes flux decline occurred after approximately 60 min of filtration (**Figure 4a**). The delay in the onset of flux decline

was attributed to a variety of factors. To observe flux decline, the hydraulic resistance of the membrane and fouling layer(s) must exceed that of the virgin membrane ($R_T = R_m + R_{fouling}$). Therefore, the delay in observed flux loss was indicative of the dynamic formation of the membrane fouling mechanism(s). Differences in flux loss at the termination of the filtration period are indicative of differences in the affinity of the membrane surface for the specific foulant, which in this case was the mineral oil, surface coverage and the extent of pore blocking that has occurred. For the mineral oil the PANI_PAN membrane demonstrated the lowest affinity for, or highest resistant, adhesion for the mineral oil. All PAN membranes had a high rejection efficiency for the mineral oil with turbidity rejection ≥99% (~100 NTU to ≤0.1 NTU) over the entire filtration periods (**Figure 4b**). The relative stability of the oil rejection suggested that a homogeneous secondary membrane did not form on the membrane surface, which would have resulted in increased oil rejection, and that oil deformation and breakthrough through the pore throats did not (substantially) occur.

(a)

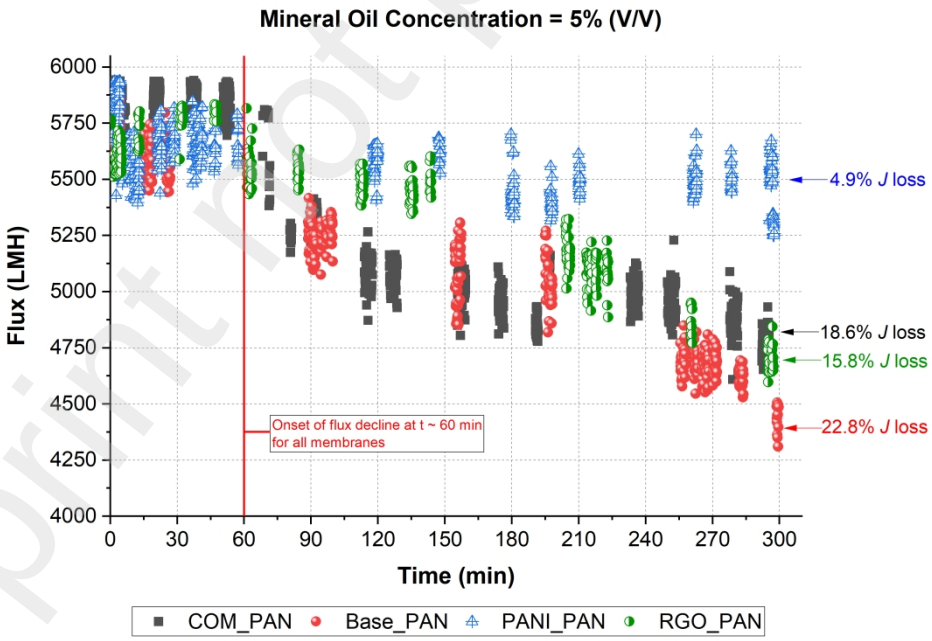

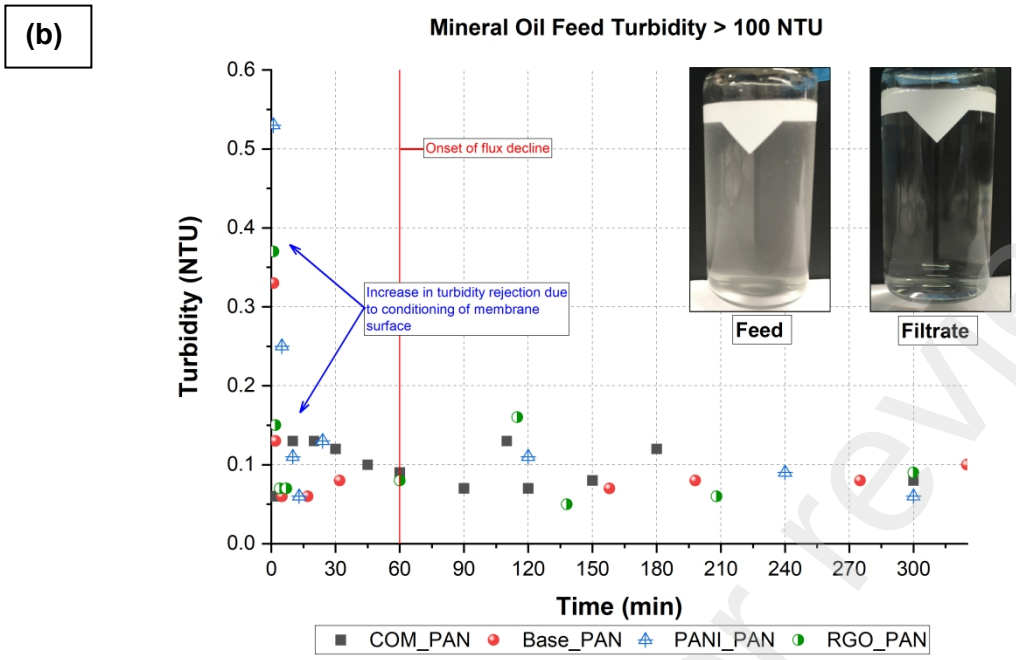

Figure 4. (a) Water flux as a function of time for the PAN membranes treating a 5% v/v mineral oil emulsion in a simple electrolyte solution ($P = 0.35\ bar$, TDS=20,000 mg/L NaCl, pH=7, T=20ºC). (b) Filtrate turbidity as a function of filtration time for the studied PAN membranes treating the mineral oil emulsion.

Similar to the mineral oil results, the PANI_PAN membrane was characterized as the most resistant to flux decline (fouling) by the toluene emulsion folowed by the Base_PAN, RGO_PAN, and COM_PAN membranes, respectively (**Figure 5a**). The COM_PAN experienced rapid, and severe, flux loss as a result of toluene fouling at the onset of emulsion filtration (~3 min). Rapid flux loss did not occur until 45 min after initiation of filtration for the Base_PAN and PANI_PAN membranes, and at 20 min for the RGO_PAN membrane. Rapid flux decline for the PANI_PAN membrane did in fact not occur until 30 min after the toluene concentration was increased from 1% to 2% V/V. This would suggest that fouling for the PANI_PAN membrane was primarily through semi-permiable gel formation on the membrane surface rather than pore constriction/plugging as these mechanisms are associated with rapid flux decline. The differences

in the times required for rapid fouling to occur were due to differences in the affinity of the toluene droplets with the respective membrane surfaces. As was the case for the mineral oil tests the filtrate turbidity remained constant for each fo the membranes over the studied filtration period (**Figure 5b**) suggesting that breakthrough was not occurring.

(a)

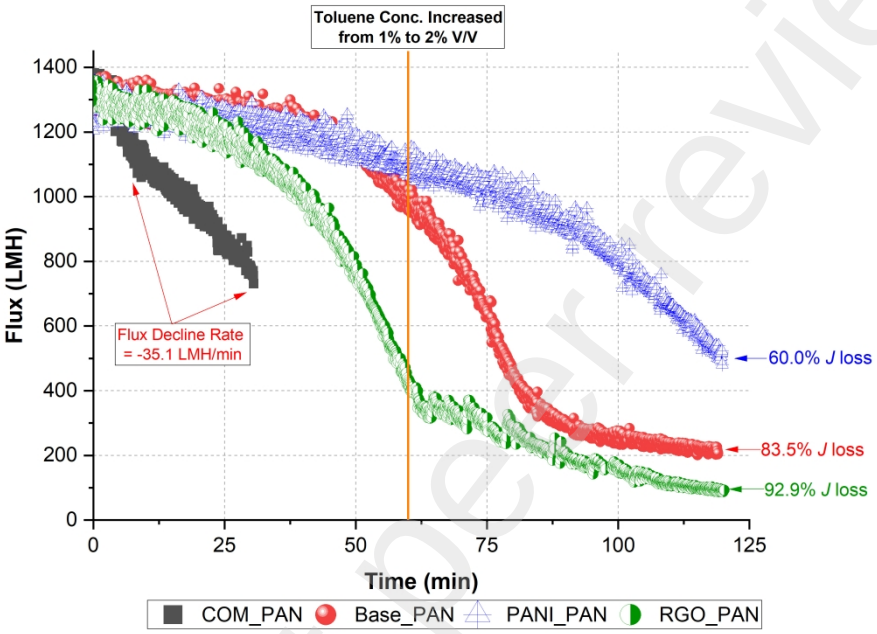

(b)

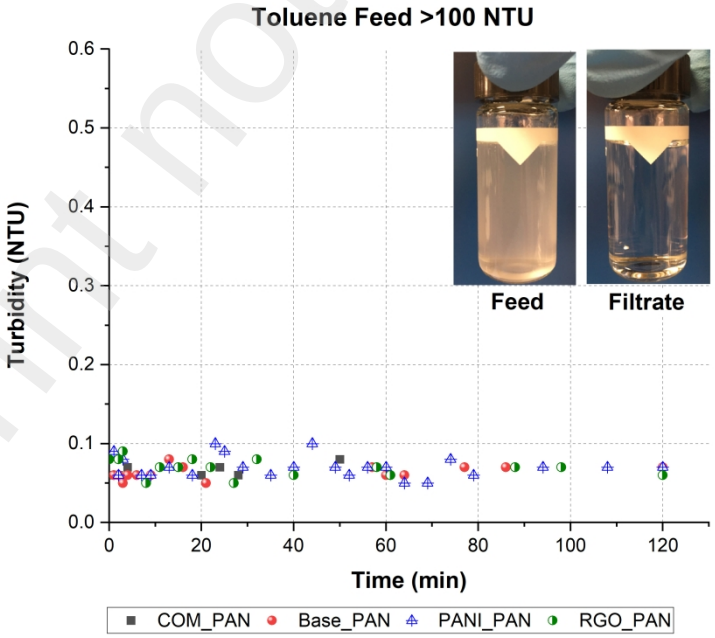

Figure 5. (a) Water flux as a function of time for the PAN membranes treating 1% and 2% V/V toluene emulsions in a simple electrolyte solution ($P = 0.35\ bar$, TDS=20,000 mg/L NaCl, *T*=20°C, pH=7). (b) Filtrate turbidity as a function of filtration time for the studied PAN membranes treating the toluene emulsion.

As was the case for the mineral oil and toluene performance trials, the PANI_PAN membrane outperformed the COM_PAN and other nanofibrous membranes in the benzene trials (**Figure 6**). Unlike the other membranes the PANI_PAN membrane was not characterized by rapid flux decline over the filtration period (**Figure 6a**). The COM_PAN, Base_PAN, and RGO_PAN membranes all experienced rapid flux decline after approximately 12 min after initiation of filtration. This time period was slightly extended for the RGO_PAN and Base_PAN membranes relative to the COM_PAN; however, at this time these membranes all had similar rates of flux decline leading to terminal flux loss at around 90 min. As was observed for the other emulsions the filtrate turbity remained relatively constant (**Figure 6b**) for each fo the PAN membranes, indicating good separation of the benzene.

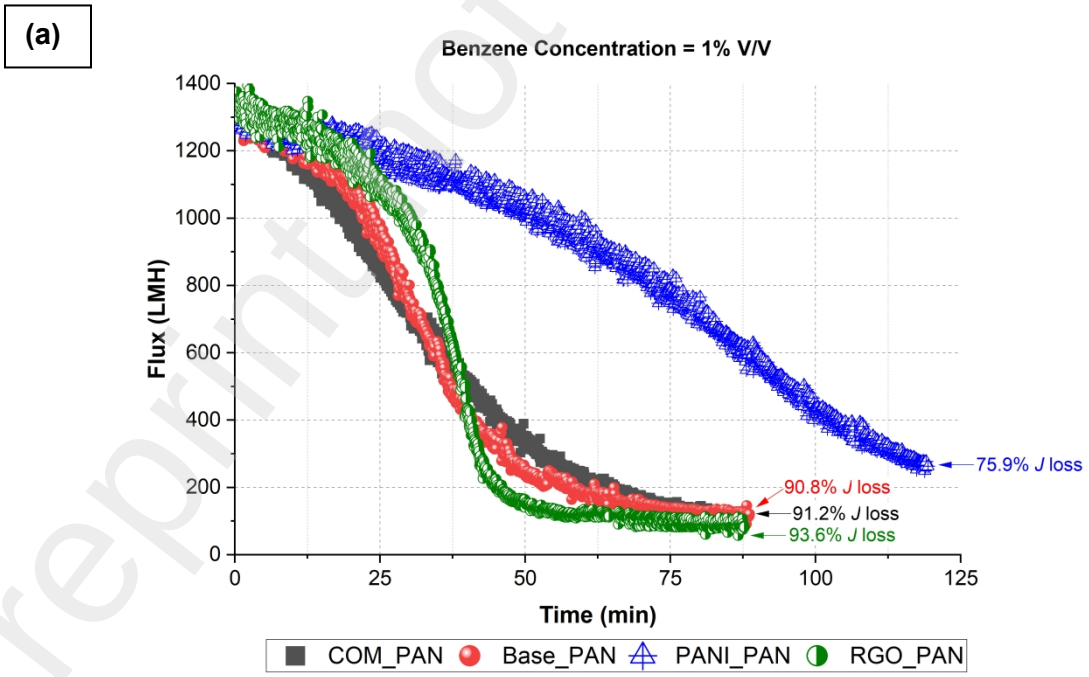

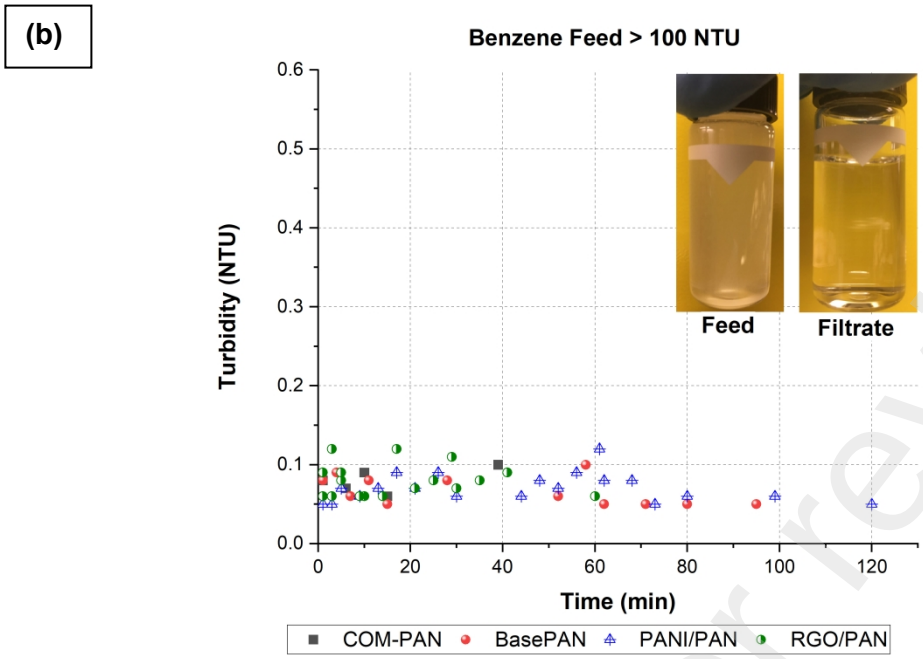

460 **Figure 6.** Water flux as a function of time for the PAN membranes treating 1% V/V benzene
461 emulsions in a simple electrolyte solution ($P = 0.35\ bar$, TDS=20,000 mg/L NaCl, *T*=20°C,
462 pH=7). (b) Filtrate turbidity as a function of filtration time for the studied PAN membranes
463 treating the benzene emulsion.

464 The contact angles, or affinities, of the oil/solvent phases with the membranes are shown in
465 **Figure 7a.** These values were used to calculate the hydraulic pressure required (**Eq. 4**) for a
466 given phase to enter the pore throats of the tested membranes and is reported as a function of
467 droplet size in **Figure 7b-d**. The relationship between phase entry pressure and the droplet
468 diameter that may enter a given pore throat was logarithmic for each case. At the hydraulic feed
469 pressure used in the cross-flow tests there was little differentiation between the commercially
470 available and nanofibrous PAN membranes in terms of the droplet diameter limit at which entry
471 into the pore throats would occur. This cutoff was between 0.7 to 0.8 μm for all of the tested
472 solvents/oils. This value is smaller than the mean sizes of the emulsions, which ranged from 1 to
473 10 μm; however, a distribution in droplet sizes were present in each of the emulsions which were
474 capable of deformation once deposited onto the membrane because of filtrate drag forces acting

on them. The differences in the phase entry pressures for the membranes becomes more evident as the feed pressure acting on the emulsion increases. The PANI_PAN membrane presented the highest resistance to droplet(s) entry into the pore network, followed by the RGO_PAN, Base_PAN and COM_PAN membranes, respectively for mineral oil (**Figure 7b**). For toluene (**Figure 7c**), the PANI_PAN membrane was followed by the COM_PAN, Base_PAN, and RGO_PAN membranes, respectively. For benzene (**Figure 7d**), the PANI_PAN membrane was like the COM_PAN and followed by RGO_PAN and Base_PAN membranes, respectively. The phase entry pressure calculations support the antifouling behavior and slower flux decline of the PANI_PAN findings from the oil/solvent flux tests.

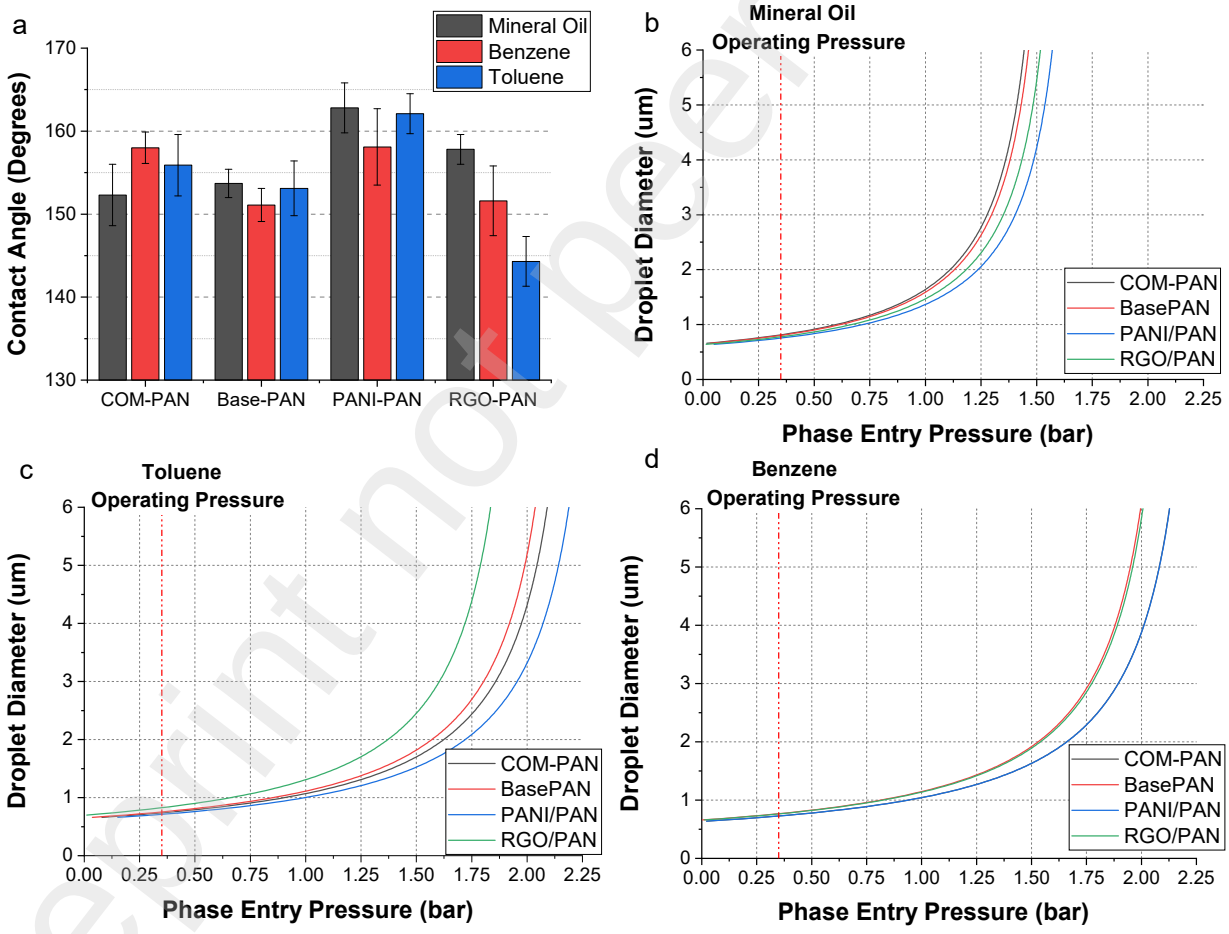

Figure 7. (*a*) Oil/solvent captive bubble in water on membrane ($\boldsymbol{V_D = 2\mu L}$; *T*=20°C, *n*=5). Phase entry pressure for the (b) mineral oil, (c) toluene, and (d) benzene emulsions for the studied PAN membranes.

Emulsions can deform to penetrate pore sizes smaller than that of the droplet, or it can coalesce into larger droplets that favor detachment from the membrane [11] as illustrated in **Figure S4.** The behavior of the emulsion at the membrane surface is largely a function of the membrane's affinity (adhesion) for the emulsion [11]. For the mineral oil, the Base_PAN membrane was characterized by extensive surface coverage and penetration into the fibrous structure (**Figure 8**). Conversely, the coverage and penetration were less extensive for the RGO_PAN and PANI_PAN membranes. The PANI_PAN had a low affinity for mineral oil (θ_{OW} =163°) and showed the greatest resistance to oil fouling. The RGO_PAN membrane also had a low affinity for the mineral oil, relative to that measured for the other PAN membranes (**Figure 7a**). Therefore, mineral oil was likely coalescing and detaching from the PANI_PAN and RGO_PAN membrane surfaces. The interpretation of toluene and benzene fouling was more difficult because of solvent evaporation prior to autopsy; however, the PANI-PAN membrane was characterized by fewer gel-like surface deposits after the toluene and benzene tests when compared to the Base_PAN and RGO_PAN membranes (**Figure 8**). This is supported by the contact angles between the benzene and toluene on the Base_PAN and RGO_PAN membranes (**Figure 7a**), which were less than that of the PANI_PAN indicating a more favorable adhesion with these solvents. This would suggest that both the toluene and benzene were more easily removed by shear forces on the PANI_PAN membrane compared to its counterpart membranes. This observation supports the membrane fouling results where the PANI_PAN membranes were subject to less severe flux decline that the Base_PAN and RGO_PAN membranes.

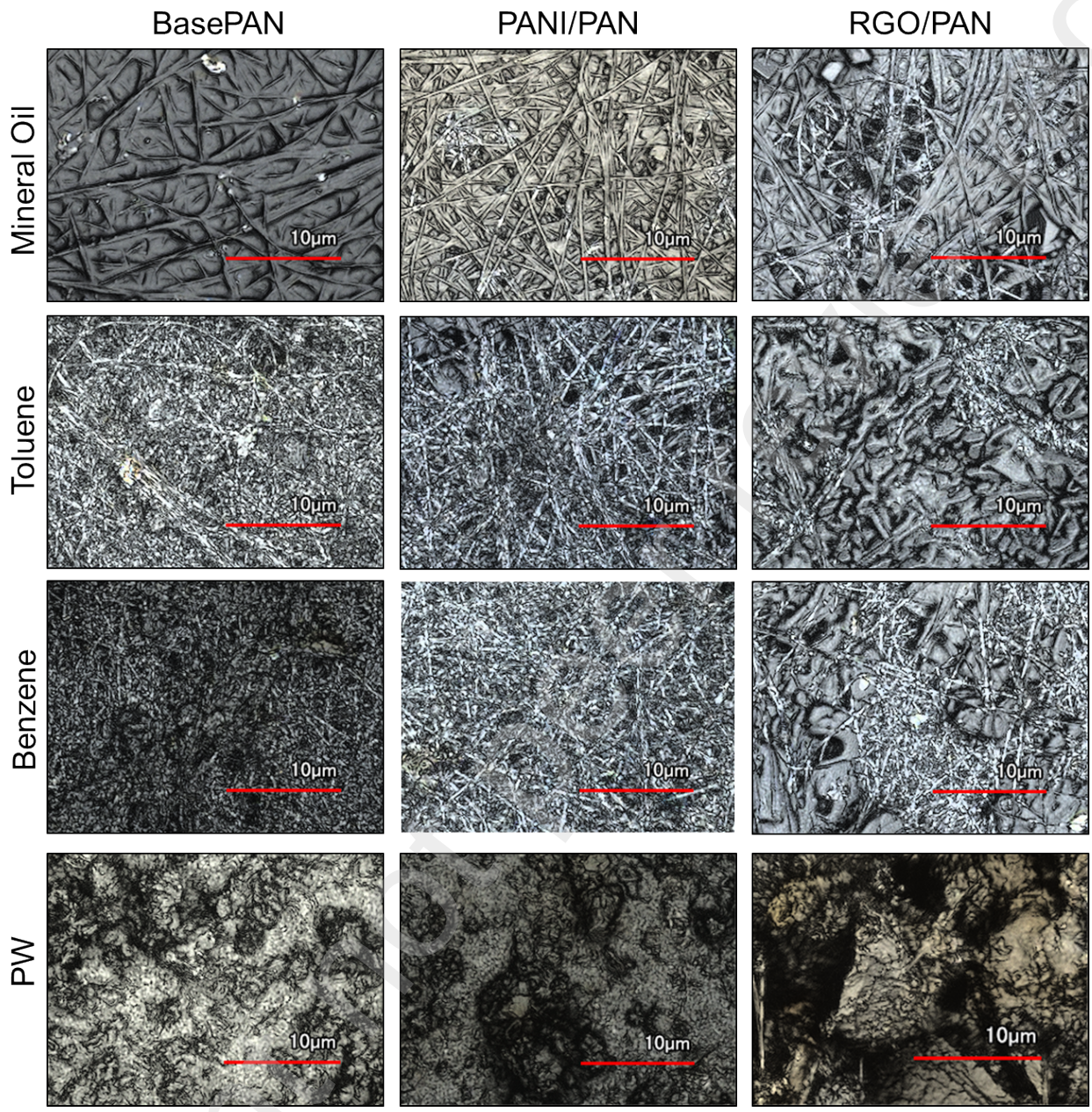

Figure 8. Representative images of the synthesized PAN membranes after each of the oil/solvent emulsion and PW fouling tests. Images were collected using a laser microscope.

4.2.2 PW Performance and Fouling

Water flux as a function of filtration time for the membranes treating the PW are summarized in **Figure 9a**. All membranes showed a time delay before rapid flux decline, as was also observed for the mineral oil separation tests (**Figure 4**). This time delay was considered to represent the

time for a conditioning layer to have formed and/or for pore constriction/plugging to become substantial. These delays were longest for the RGO_PAN (15 mins), PANI_PAN (11 mins) and Base_PAN (8 mins) membranes. Rapid flux loss occurred almost immediately (4 mins) for the COM_PAN. The RGO/PAN membrane demonstrated the least amount of flux loss (76%) after 60 mins of filtration. The average ending flux for the RGO/PAN membrane was 300 LMH at a back pressure of 0.35 bar (permeance = 857 LMH/bar). The PANI/PAN membrane demonstrated the second least amount of flux loss (86%) after 60 mins of filtration. The average ending flux for the PANI_PAN membrane was 190 LMH at a back pressure of 0.35 bar (permeance = 486 LMH/bar). The less steep flux decline curves observed for the RGO/PAN and PANI/PAN, relative to the other membranes, indicated a lower affinity of the foulants (oils and greases, TSS) for the membrane surface resulting is slower conditioning of the membrane surface. After the rapid flux decline, the flux for all membranes approached a steady-state value after approximately 55 mins of filtration.

Turbidity was reduced from ~31 NTU to <0.6 NTU for all membranes with rejection increasing as filtration progressed, ultimately reaching steady-state values after 10 min of filtration (**Figure 9b**). While the PANI_PAN and RGO_PAN membranes showed high rejection (<0.3 NTU) from the start of the test, the COM_PAN and Base_PAN membranes initially showed higher turbidity break through at 0.55 NTU and 0.43 NTU, respectively. The higher initial turbidity values seen from the COM_PAN and Base_PAN show that the membrane went through a conditioning period where small amount of breakthrough occurred. As the cake layer grew on the membrane surface, the rejection increased and stayed steady for the remainder of the test. Neither RGO_PAN nor PANI_PAN showed significant breakthrough during the membrane conditioning period. Surface caking was evidenced for each of the membranes after PW filtration (**Figure 10**). The appearance of the cake layer was characterized as a greasy clay layer. From these photos, the PANI_PAN membrane showed evidence of cake layer sluffing down the center of the flow channel where the crossflow velocity was at its greatest due to the parabolic flow velocity that exists in a channel.

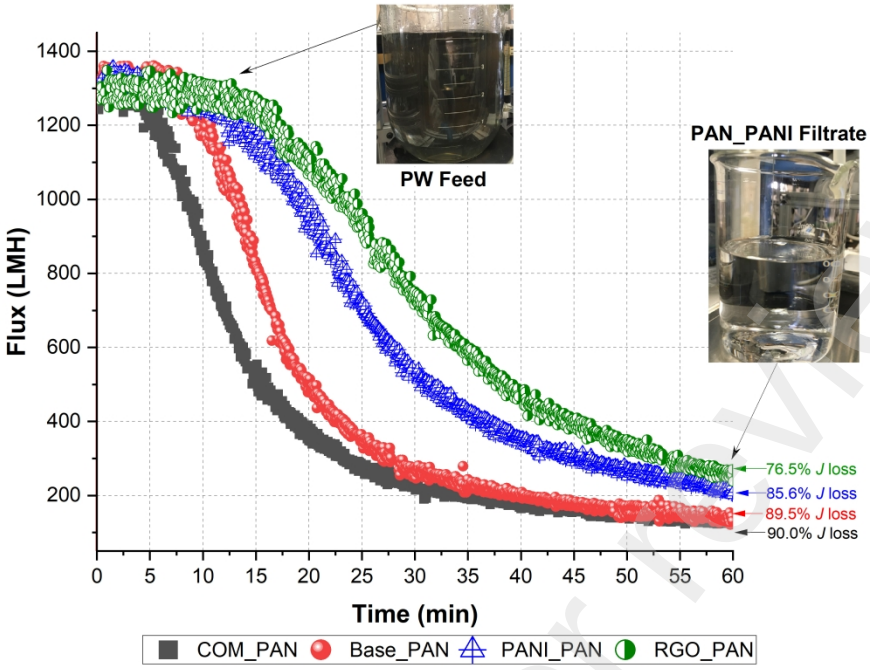

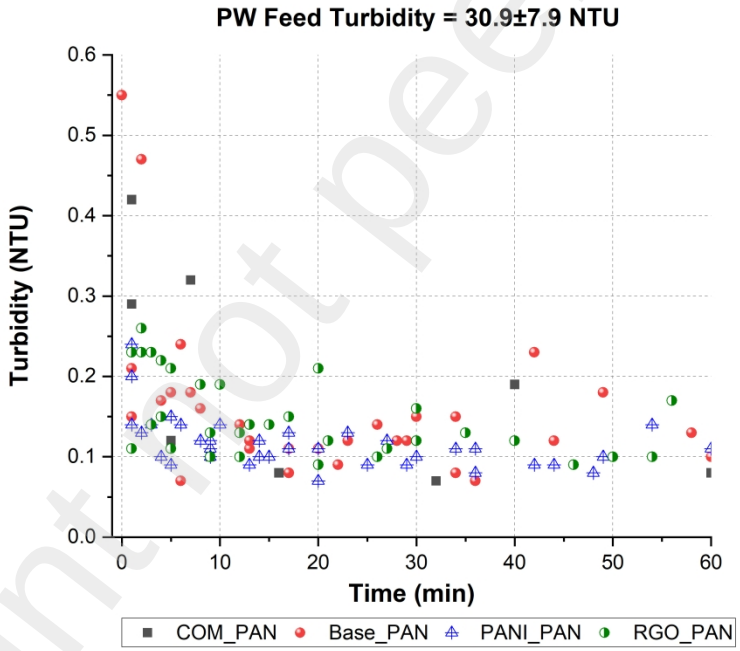

Figure 9. Flux decline curves, percent flux loss, and filtrate turbidity for PW tests. Table values represent the average of three runs per membrane. ($\boldsymbol{P = 0.35\ bar}$, TSS=172 mg/L, TDS≈76,000 mg/L, Total O&G≈4,500 mg/L, pH=7.5, *T*=20°C)

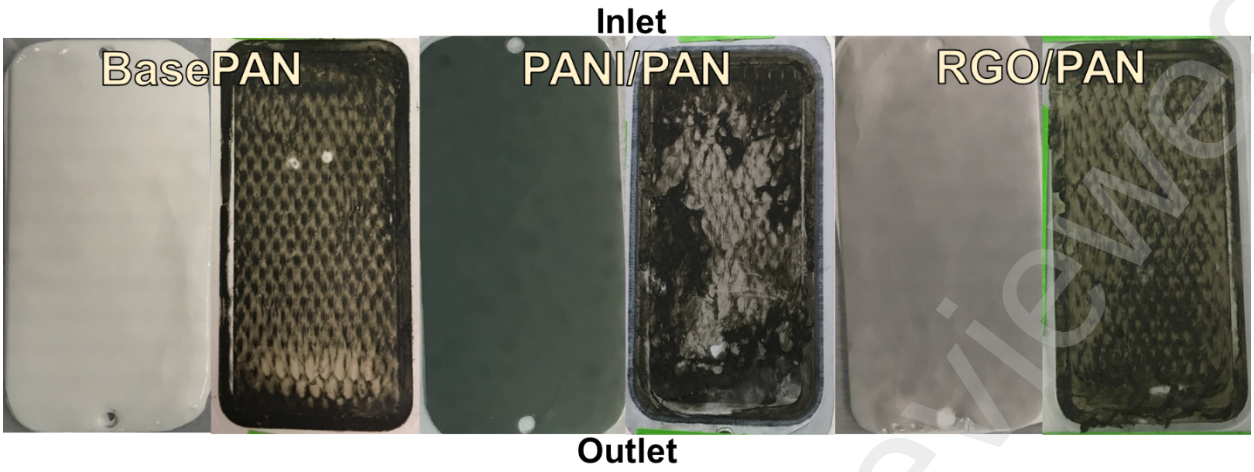

Figure 10. For each membrane set, the left membrane shows before test and the left membrane shows fouling post PW test

The fouling characteristics of the studied membranes may be distinguished based on porosity and oleophobicity. Hydrophilicity and MFP were all statistically similar and do not appear to be significantly distinguishing characteristics. All the electrospun membranes had higher porosities than did the COM_PAN (**Table 1**), which consistently suffered more rapid and severe flux loss. The higher porosities would allow for the membranes to compensate when portions of flow paths/pore throats become constricted or blocked. In other words, the more substantial pore space requires greater surface coverage to achieve a given flux decline rate and loss. Secondly, the interfacial chemistry between the membrane and the non-aqueous phases were important. Although the water contact angles were similar, the PANI_PAN had the highest oil/solvent contact angles (**Figure 7a**) indicative of a lower affinity for the non-aqueous phases relative to the other membranes. Consequently, it demonstrated a greater resistance to fouling for the tested emulsions. Although the amino groups on the PANI did not increase the PANI_PAN hydrophilicity compared to the Base_PAN, they did increase its oleophobicity. A more complex picture arises when treating the PW studied here. Because there is a diversity of substances in the PW, including solvents and oils, clear correlations of membrane surface chemistry and fouling behavior cannot be drawn; however, the higher porosities of the electrospun membranes continued to

prove desirable. Therefore, the higher membrane porosities that may be achieved through electrospinning present a clear advantage over conventionally made membranes.

5. CONCLUSIONS

Electrospun PAN membranes presented superior water permeance and fouling (non-aqueous substances) resistance characteristics to a commercially made PAN membrane in realistic crossflow configurations. These improvements were attributed to a combination of higher membrane porosity (primary) and greater oleophobicity (secondary). These differences in surface chemical and physical properties translated to higher efficiencies when treating a complex feed solution, in this case a PW. Nanoparticles may be successfully integrated into nanofibrous membranes to create fouling resistant membranes for PW applications, though aggregation within the polymer solution must be carefully controlled to prevent defect formation.

ACKNOWLEDGEMENTS

This work was supported by the U.S. Department of Energy, Office of Fossil Energy, and National Energy Technology Laboratory (NETL) under Award Number DE-FE0031855. We also gratefully acknowledge the support of Ralph DiPalma and Neenah Filtration for providing the Cranemat membrane support material.

REFERENCES

1. Al-Ghouti, M.A., et al., *Produced water characteristics, treatment and reuse: A review.* Journal of Water Process Engineering, 2019. **28**: p. 222-239.

2. Veil, J., *U.S. Produced Water Volumes and Management Practices in 2017*. 2020, Veil Environmental, LLC.

3. Boysen, D.B., J.E. Boysen, and J.A. Boysen, *Strategic Produced Water Management and Disposal Economics in the Rocky Mountain Region*. 2000, BC Technologies, Ltd. p. 12.

4. Benko, K.L. and J.E. Drewes, *Produced Water in the Western United States: Geographical Distribution, Occurrence, and Composition.* Environmental Engineering Science, 2008. **25**(2): p. 239-246.

5. Abd Halim, N.S., et al., *Recent Development on Electrospun Nanofiber Membrane for Produced Water Treatment: A review.* Journal of Environmental Chemical Engineering, 2021. **9**(1).

6. Zaidi, A., K. Simms, and S. Kok, *The Use of Micro/Ultrafiltration for the Removal of Oil and Suspended Solids from Oilfield Brines.* Water Science and Technology, 1992. **25**(10): p. 163-176.

7. Santos, S.M. and M.R. Wiesner, *Ultrafiltration of water generated in oil and gas production.* Water Environment Research, 1997. **69**(6): p. 1120-1127.

8. Mokarizadeh, H. and A. Raisi, *Industrial wastewater treatment using PES UF membranes containing hydrophilic additives: Experimental and modeling of fouling mechanism.* Environmental Technology & Innovation, 2021. **23**.

9. Song, C. and G.C. Rutledge, *Electrospun polyimide fiber membranes for separation of oil-in-water emulsions.* Separation and Purification Technology, 2021. **270**.

10. Huang, S., R.H.A. Ras, and X. Tian, *Antifouling membranes for oily wastewater treatment: Interplay between wetting and membrane fouling.* Current Opinion in Colloid & Interface Science, 2018. **36**: p. 90-109.

11. Tummons, E.N., et al., *Behavior of oil droplets at the membrane surface during crossflow microfiltration of oil–water emulsions.* Journal of Membrane Science, 2016. **500**: p. 211-224.

12. Tummons, E.N., et al., *Ultrafiltration of saline oil-in-water emulsions stabilized by an anionic surfactant: Effect of surfactant concentration and divalent counterions.* Journal of Membrane Science, 2017. **537**: p. 384-395.

13. He, Z., et al., *The effect of permeate flux on membrane fouling during microfiltration of oily water.* Journal of Membrane Science, 2017. **525**: p. 25-34.

14. Tanudjaja, H.J., et al., *Effect of cross-flow velocity, oil concentration and salinity on the critical flux of an oil-in-water emulsion in microfiltration.* Journal of Membrane Science, 2017. **530**: p. 11-19.

15. Tanudjaja, H.J. and J.W. Chew, *Assessment of oil fouling by oil-membrane interaction energy analysis.* Journal of Membrane Science, 2018. **560**: p. 21-29.

16. Otitoju, T.A., A.L. Ahmad, and B.S. Ooi, *Polyvinylidene fluoride (PVDF) membrane for oil rejection from oily wastewater: A performance review.* Journal of Water Process Engineering, 2016. **14**: p. 41-59.

17. Koltuniewicz, A.B., R.W. Field, and T.C. Arnot, *Cross-flow and dead-end microfiltration of oily-water emulsion. Part I: Experimental study and analysis of flux decline.* Journal of Membrane Science, 1995. **102**: p. 193-207.

18. Tanudjaja, H.J. and J.W. Chew, *Critical flux and fouling mechanism in cross flow microfiltration of oil emulsion: Effect of viscosity and bidispersity.* Separation and Purification Technology, 2019. **212**: p. 684-691.

19. Zarghami, S., et al., *Superhydrophilic and underwater superoleophobic membranes - A review of synthesis methods.* Progress in Polymer Science, 2019. **98**.

20. Otitoju, T.A., A.L. Ahmad, and B.S. Ooi, *Superhydrophilic (superwetting) surfaces: A review on fabrication and application.* Journal of Industrial and Engineering Chemistry, 2017. **47**: p. 19-40.

21. Drelich, J. and E. Chibowski, *Superhydrophilic and superwetting surfaces: definition and mechanisms of control.* Langmuir, 2010. **26**(24): p. 18621-3.

22. Brant, J.A. and A.E. Childress, *Assessing short-range membrane–colloid interactions using surface energetics.* Journal of Membrane Science, 2002. **203**(1–2): p. 257-273.

23. Tummons, E., et al., *Membrane fouling by emulsified oil: A review.* Separation and Purification Technology, 2020. **248**.

24. Huang, Y., et al., *Ultrafiltration Membranes with Structure-Optimized Graphene-Oxide Coatings for Antifouling Oil/Water Separation.* Advanced Materials Interfaces, 2015. **2**(2).

25. Su, R., et al., *Recent progress in electrospun nanofibrous membranes for oil/water separation.* Separation and Purification Technology, 2021. **256**.

26. Du, C., et al., *One-step electrospinning PVDF/PVP-TiO2 hydrophilic nanofiber membrane with strong oil-water separation and anti-fouling property.* Colloids and Surfaces A: Physicochemical and Engineering Aspects, 2021. **624**.

27. Faraji, M., S.R. Nabavi, and H. Salimi-Kenari, *Fabrication of a PAN–PA6/PANI membrane using dual spinneret electrospinning followed by in situ polymerization for separation of oil-in-water emulsions.* New Journal of Chemistry, 2020. **44**(31): p. 13488-13500.

28. Taylor, G.I., *Electrically diven jets.* Proc Roy Soc, 1969(313): p. 453-75.

29. Zhang, J., et al., *Antifouling hydrolyzed polyacrylonitrile/graphene oxide membrane with spindle-knotted structure for highly effective separation of oil-water emulsion.* Journal of Membrane Science, 2017. **532**: p. 38-46.

30. Shakiba, M., et al., *Development of a superhydrophilic nanofiber membrane for oil/water emulsion separation via modification of polyacrylonitrile/polyaniline composite.* Polymers for Advanced Technologies, 2020. **32**(3): p. 1301-1316.

31. Zhang, J., et al., *Graphene oxide/polyacrylonitrile fiber hierarchical-structured membrane for ultra-fast microfiltration of oil-water emulsion.* Chemical Engineering Journal, 2017. **307**: p. 643-649.

32. Liu, M., et al., *Stable underwater superoleophobic conductive polymer coated meshes for high-efficiency oil–water separation.* RSC Advances, 2015. **5**(42): p. 33077-33082.

33. Karbownik, I., et al., *The Preparation and Characterization of Polyacrylonitrile-Polyaniline (PAN/PANI) Fibers.* Materials (Basel), 2019. **12**(4).

34. Zhai, G., et al., *Conductive composite films composed of polyaniline thin layers on microporous polyacrylonitrile surfaces.* Thin Solid Films, 2010. **519**(1): p. 169-173.

35. Krishnamoorthy, K., et al., *The chemical and structural analysis of graphene oxide with different degrees of oxidation.* Carbon, 2013. **53**: p. 38-49.

36. Singh, R. and C. Charu Tripathi, *Enhancing Graphene Concentration in Organic Solvents with Salts and Additives.* Materials Today: Proceedings, 2018. **5**(1): p. 1455-1461.

37. Konios, D., et al., *Dispersion behaviour of graphene oxide and reduced graphene oxide.* J Colloid Interface Sci, 2014. **430**: p. 108-12.

671 38. Dang, T.T., et al., *Superior dispersion of highly reduced graphene oxide in N,N-*
672 *dimethylformamide.* J Colloid Interface Sci, 2012. **376**(1): p. 91-6.

673 39. Naseeb, N., et al., *A Novel PAN-GO-SiO(2) Hybrid Membrane for Separating Oil and*
674 *Water from Emulsified Mixture.* Materials (Basel), 2019. **12**(2).

675 40. Yang, G.Z., et al., *Influence of Working Temperature on The Formation of Electrospun*
676 *Polymer Nanofibers.* Nanoscale Res Lett, 2017. **12**(1): p. 55.

677 41. Szewczyk, P.K. and U. Stachewicz, *The impact of relative humidity on electrospun*
678 *polymer fibers: From structural changes to fiber morphology.* Adv Colloid Interface Sci,
679 2020. **286**: p. 102315.

680 42. Flint, L.E. and A.L. Flint, *2.3 Porosity*, in *Methods of Soil Analysis*. 2002. p. 241-254.

681 43. van Oss, C.J., *Interfacial Forces in Aqueous Media*. 2nd ed. 2006: CRC Press.

682 44. Jepsen, K., et al., *Membrane Fouling for Produced Water Treatment: A Review Study*
683 *From a Process Control Perspective.* Water, 2018. **10**(7).

684 45. Darvishzadeh, T. and N.V. Priezjev, *Effects of crossflow velocity and transmembrane*
685 *pressure on microfiltration of oil-in-water emulsions.* Journal of Membrane Science, 2012.
686 **423-424**: p. 468-476.

687 46. Zhang, X., et al., *Interfacial characteristics in membrane filtration for oil-in-water treatment*
688 *processes.* Journal of Membrane Science, 2021. **623**.

689 47. Nazzal, F.F. and M.R. Wiesner, *Microfiltration of Oil-in-Water Emulsions.* Water
690 Environment Research, 1996. **68**(7): p. 1187-1191.

48. Nezarati, R.M., M.B. Eifert, and E. Cosgriff-Hernandez, *Effects of humidity and solution viscosity on electrospun fiber morphology.* Tissue Eng Part C Methods, 2013. **19**(10): p. 810-9.

49. Zhang, F., et al., *Alkaline-induced superhydrophilic/underwater superoleophobic polyacrylonitrile membranes with ultralow oil-adhesion for high-efficient oil/water separation.* Journal of Membrane Science, 2016. **513**: p. 67-73.

EMULSION SEPARATION AND FOULING OF ELECTROSPUN POLYACRYLONITRILE MEMBRANES FOR PRODUCED WATER APPLICATIONS

Separation and Purification Technology

Supplementary Information

Elizabeth M. Butler [1] and Jonathan A. Brant [1,*]

[1] University of Wyoming, department of Civil and Architectural Engineering and Construction Management, 1000 E. University Avenue, Laramie, WY, 82071.

* Corresponding author. Email: jbrant1@uwyo.edu.

September 13, 2022

Table S1. Summary of relevant electrospinning constraints and solution properties for the synthesized PAN membranes.

Designation	Code	PAN to DMF Conc. (w/w%)	Coat Additive to PAN Conc. (w/w%)	Solution Viscosity @ 23°C (mPa*s)	ΔV (kV)	Spinning Temp. (°C)
	4%PAN	4	-	23	17	25/30
	6%PAN	6	-	75	16	25/30
	8%PAN	8	-	202	15	25/30
	10%PAN	10	-	601	14	25/30
	12%PAN	12	-	768	14	25/30
PAN Support	Support PAN	12	0	768	14	25
PAN Top Layer	BasePAN*	6	0	75	16	30
PANI Top Layer	PANI/PAN*	6	30	77	16	30
RGO Top Layer	RGO/PAN*	6	7	77	16	30
*The designations of BasePAN, PANI/PAN, and RGO/PAN will refer to the total membrane containing Support PAN and top layer						

Table S2. Surface energy/tension (mJ/m^2) components of relevant solvents and oils used in this study (T=20°C) [43]

Liquid	ρ(g/mL)	μ (mP*s)	γ_{total}	γ_{LW}	$\gamma+$	$\gamma-$	γ_{AB}	γ_{WO} (N/m)
Water	0.9982	1.00	72.8	21.8	25.5	25.5	51.0	-
Benzene	0.879	0.649	28.58	28.58	0	0	35	35
Toluene	0.869	0.583	28.3	28.3	0	0	36.1	35
Mineral Oil	0.83*	2.45*	~30*	-	-	-	-	25

*values from manufacturer

γ_{total} = total surface/interfacial energy/tension

γ_{LW} = surface/interfacial energy/tension from dispersion forces

$\gamma+$ = surface/interfacial energy/tension from acid non-dispersion forces

$\gamma-$ = surface/interfacial energy/tension from base non-dispersion forces

γ_{WO} = surface/interfacial energy/tension between water and oil/solvent

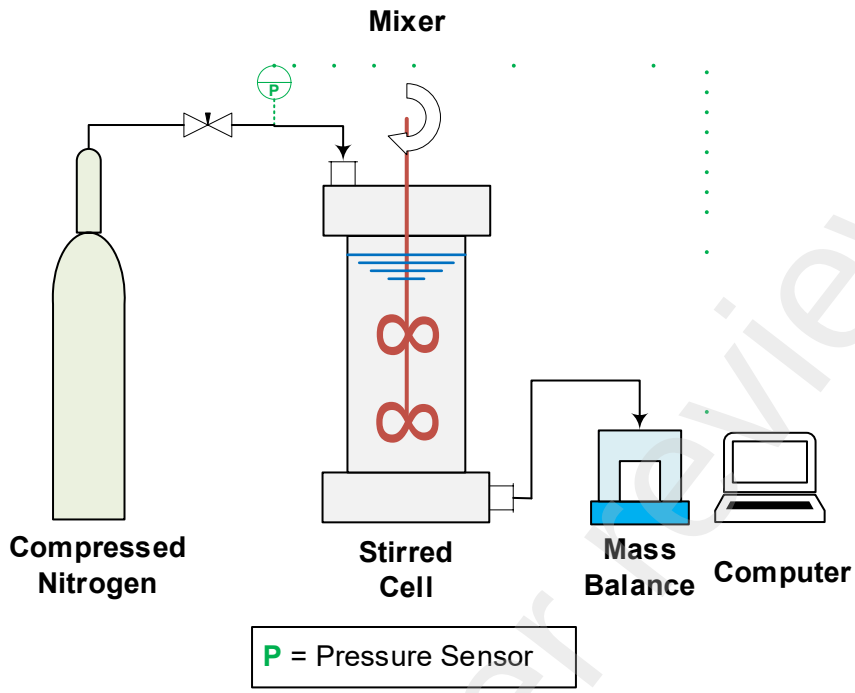

727

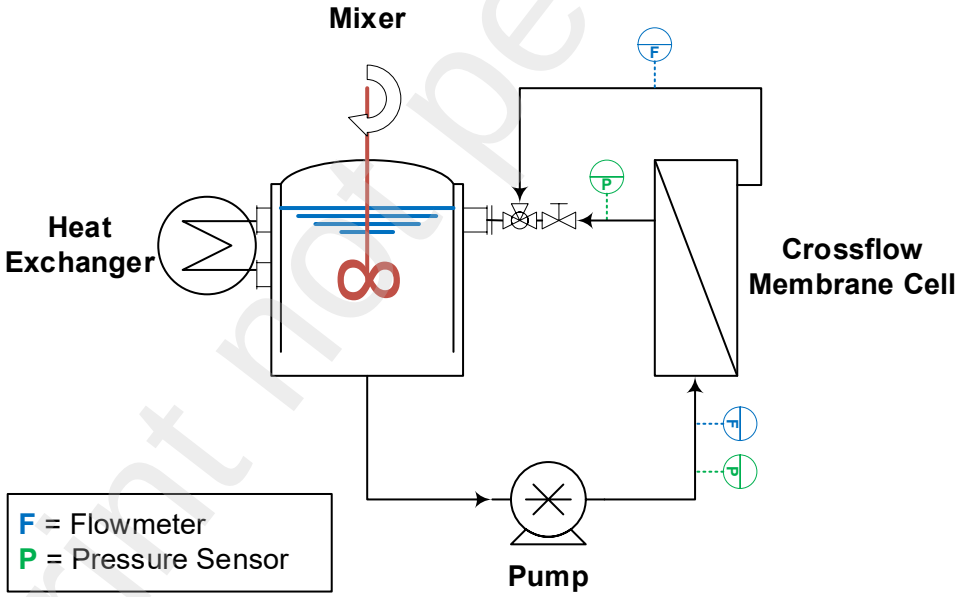

728

729 **Figure S1**. (*top*) Process flow diagram for the dead-end filtration apparatus used for
730 characterizing water permeance. (*bottom*) Process flow diagram for the crossflow test unit used
731 for evaluating membrane fouling and water flux over time.

732

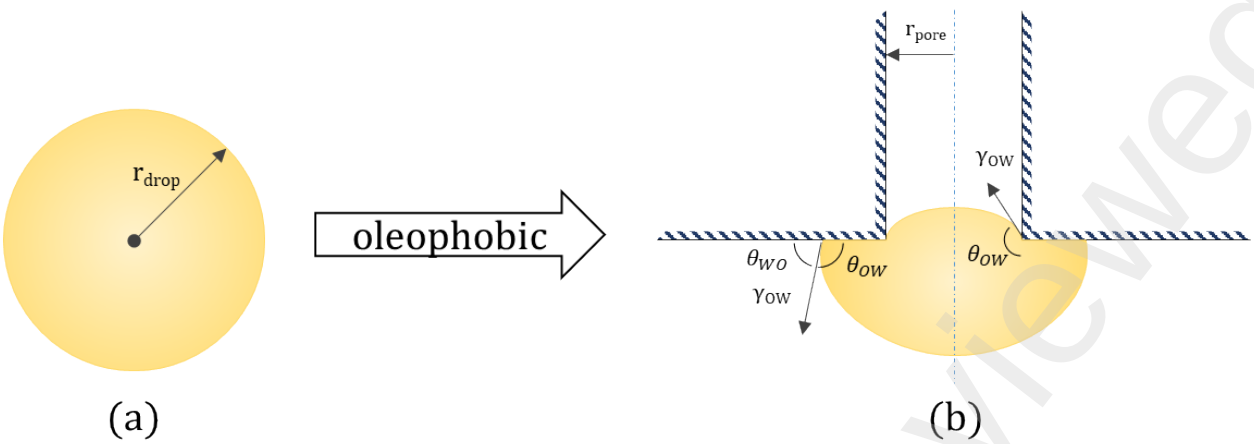

733

734 **Figure S1.** Schematic of a static oil droplet (*a*) on an oleophobic pore (*b*). Important dimensions
735 include the radius of the oil droplet, $\boldsymbol{r_{drop}}$, the radius of the membrane pore, $\boldsymbol{r_{pore}}$, the contact
736 angle of oil on the membrane surface in water, $\boldsymbol{\theta_{OW}}$, and the contact angle of the water on the
737 membrane surface in the presence of oil droplet, $\boldsymbol{\theta_{WO}}$ where $\boldsymbol{\theta_{WO}} + \boldsymbol{\theta_{OW}} = 180°$

738

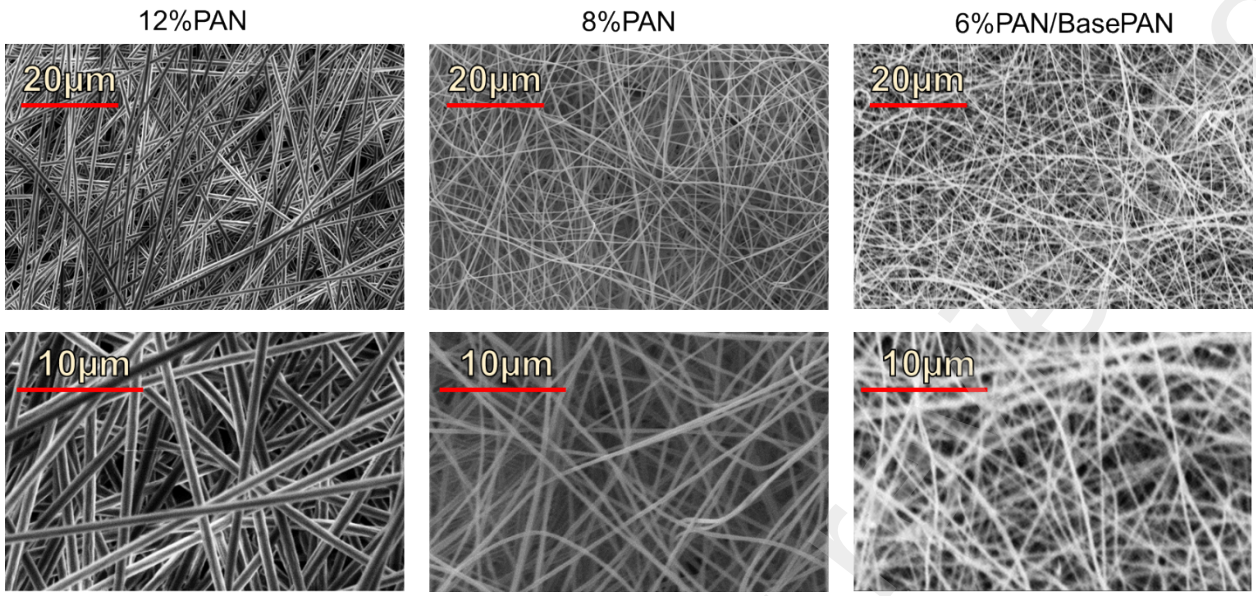

739

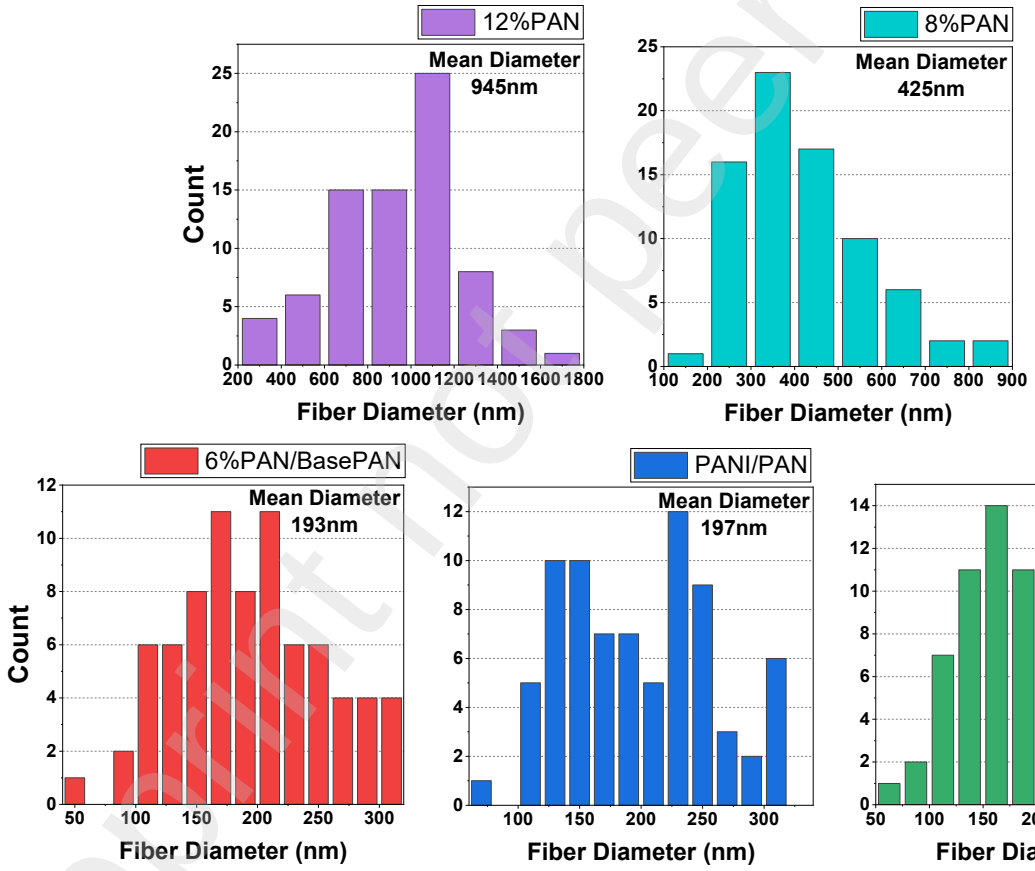

740

741 **Figure S3.** (*top*) Representative FESEM images of the 12% PAN, 8% PAN, and 6% PAN
742 (Base_PAN) nanofibrous membranes showing reductions in nanofiber diameter with decreasing
743 polymer concentration in the electrospinning solution. (*bottom*) Histogram of nanofiber
744 diameters for 12% PAN, 8% PAN, 6% PAN, PANI/PAN, and RGO/PAN.

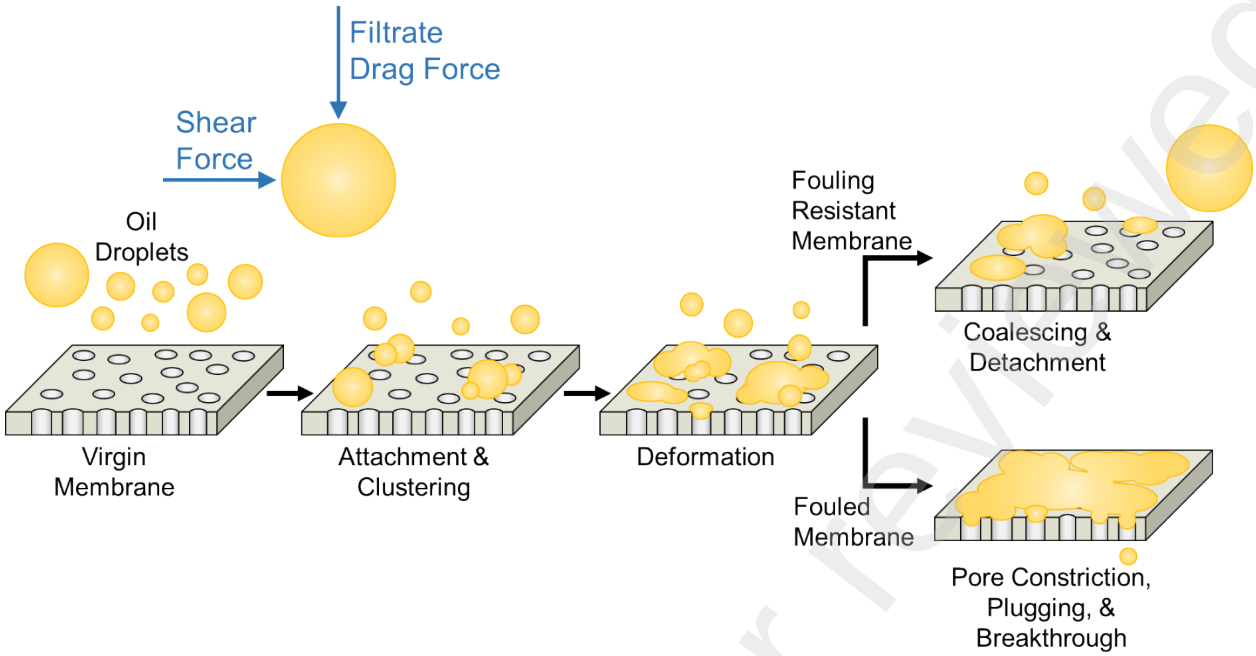

745

746 **Figure S4**. Illustration of potential oil fouling mechanisms for microporous membranes.